

Edges and Endpoints in 21-cm Observations from Resonant Photon Production

Andrea Caputo^{1,*}, Hongwan Liu^{2,3,†}, Siddharth Mishra-Sharma^{2,‡}, Maxim Pospelov^{4,5},
Joshua T. Ruderman^{2,6,§} and Alfredo Urbano^{7,8,||}

¹*Instituto de Física Corpuscular, CSIC-Universitat de Valencia, Apartado de Correos 22085, E-46071, Spain*

²*Center for Cosmology and Particle Physics, Department of Physics, New York University,
New York, New York 10003, USA*

³*Department of Physics, Princeton University, Princeton, New Jersey 08544, USA*

⁴*School of Physics and Astronomy, University of Minnesota, Minneapolis, Minnesota 55455, USA*

⁵*William I. Fine Theoretical Physics Institute, School of Physics and Astronomy, University of Minnesota,
Minneapolis, Minnesota 55455, USA*

⁶*Deutsches Elektronen-Synchrotron (DESY), D-22607 Hamburg, Germany*

⁷*INFN sezione di Trieste, SISSA, via Bonomea 265, I-34132 Trieste, Italy*

⁸*IFPU, Institute for Fundamental Physics of the Universe, via Beirut 2, I-34014 Trieste, Italy*

 (Received 15 September 2020; revised 10 December 2020; accepted 25 May 2021; published 30 June 2021)

We introduce a novel class of signatures—spectral edges and end points—in 21-cm measurements resulting from interactions between the standard and dark sectors. Within the context of a kinetically mixed dark photon, we demonstrate how resonant dark photon-to-photon conversions can imprint distinctive spectral features in the observed 21-cm brightness temperature, with implications for current, upcoming, and proposed experiments targeting the cosmic dawn and the dark ages. These signatures open up a qualitatively new way to look for physics beyond the Standard Model using 21-cm observations.

DOI: [10.1103/PhysRevLett.127.011102](https://doi.org/10.1103/PhysRevLett.127.011102)

Introduction.—Observation of the redshifted 21-cm line emission from neutral hydrogen in the intergalactic medium (IGM) has recently emerged as a powerful probe of the cosmological history of our Universe. The intensity of the global 21-cm emission can be measured as the differential brightness temperature of the hydrogen spin temperature contrasted against the background radiation and scales roughly as $\Delta T_b \propto x_{\text{HI}}(1 - T_\gamma/T_s)$, where x_{HI} is the neutral hydrogen fraction, T_s is the transition spin temperature, and T_γ is the temperature of the background radiation. Its sensitive dependence on the underlying radiation fields as well as cosmic heating and ionization processes makes it a powerful probe of astrophysics as well as physics beyond the standard model (SM).

In the standard cosmological picture, the formation of the first stars and galaxies during cosmic dawn couples the spin and kinetic temperatures via the absorption and reemission of Lyman- α photons (the Wouthuysen-Field effect [1,2]), producing a distinctive absorption trough in the observed 21-cm brightness temperature as the spin temperature cools. Eventually, x-ray sources reheat the gas, and ultraviolet radiation emitted by stellar sources leads to reionization, increasing the kinetic temperature and turning off the absorption feature. At higher redshifts, radiative coupling of the spin and photon temperatures leads to $\Delta T_b \sim 0$, although the decoupling of the photon and kinetic temperatures around $z \sim 150$ and collisional coupling of the spin and kinetic temperatures leads to a minor absorption

trough around $z \sim 100$. While the depth of the absorption feature at cosmic dawn depends sensitively on the assumed astrophysics and cosmology, a bound on the maximal absorption is obtained by taking the limit of perfect coupling of the spin and kinetic temperatures and exclusively adiabatic cooling, which in the standard Λ CDM scenario corresponds to $\Delta T_b(z = 17) \approx -0.2$ K.

The EDGES experiment recently reported the measurement of the first global 21-cm signal at cosmic dawn [3], with a central value $\Delta T_b(z = 17) \simeq -0.5_{-0.5}^{+0.2}$ K at 99% confidence level which, when taken at face value, implies a disagreement with the minimum allowed value in the standard scenario. In addition to the depth, the shape of the absorption signal as measured by EDGES is unexpected as well, with the sharp turn-on and turn-off implying sudden Lyman- α injection and then sudden heating during reionization, contrary to expectation from more standard astrophysical scenarios. Taking these tensions at face value would imply the need for a modification to the standard cosmology.

We note that unmodeled foregrounds and/or systematics have been suggested as viable explanations for the unexpected features in the EDGES measurement [4–9]. While the measurement remains tentative, it provides a jumping off point for considering how signatures of new physics and nonstandard cosmology could show up in 21-cm observations.

Several mechanisms, both astrophysical and those invoking physics beyond the SM, have been proposed to explain

the EDGES observation, which would necessarily imply a larger differential in the photon and spin temperatures compared to the standard expectation [10–15]. Injection of Lyman- α photons from the most massive halos [16] and efficient star formation along with excess x-ray heating [17] are examples of nonstandard astrophysical explanations for the sharp turn-on and turn-off of the absorption feature. Mechanisms for cooling of the kinetic temperature beyond adiabatic cooling via relative velocity-dependent interaction between baryons and dark matter (DM) particles with kinetic temperature below the IGM temperature have been proposed [11], strongly constrained [12,13], and recently revived [18]. Another class of explanations relies on raising the effective radio background temperature beyond the standard temperature of the cosmic microwave background (CMB), $T_\gamma(z) = T_{\text{CMB},0}(1+z)$, where $T_{\text{CMB},0} \approx 2.725$ K is the present-day CMB temperature. In particular, Ref. [19] proposed raising the effective temperature through the production and subsequent resonant oscillation of dark photons into SM photons in the Rayleigh-Jeans (RJ) tail of the CMB. This scenario was further explored in Ref. [20] in the context of dark radiation consisting of axionlike particles (ALPs) and in Ref. [21] in the context of ALP-photon-dark photon oscillations in the presence of a primordial dark magnetic field. The basic idea is that the decay of cosmologically long-lived dark sector particles making up a large fraction of the DM density with masses in the meV range into dark photons can result in a much larger number density of dark photons in the RJ tail of the CMB as compared to regular photons. The subsequent resonant conversion of these dark photons into SM photons via a mechanism such as kinetic mixing [22] can enhance the number density of RJ photons and result in a deeper 21-cm absorption feature.

In this Letter, we study the distinctive ways resonant photon injection can imprint itself onto a measured global 21-cm signal. In particular, we showcase scenarios in which spectral features imprinted through resonant photon production can naturally explain the depth and shape of the measured EDGES absorption feature and discuss implications for constraining these scenarios with future 21-cm measurements. We describe for the first time characteristic spectral features—edges and end points—in measurements of 21-cm photons sourced during the cosmic dark ages [23–25] and originating from coupling ordinary photons to particles of the dark sector. These novel signatures have the potential to be powerful probes of physics beyond the SM. We use the *Planck* 2018 cosmology [26] throughout this work.

Spectral features due to photon injection.—Although photon injection can arise in a variety of models [19–21], for concreteness we focus on the scenario introduced in Ref. [19] where a cosmologically long-lived dark sector particle a of mass m_a with lifetime τ_a decays into dark photons A' of mass $m_{A'}$ through $a \rightarrow A'A'$, which

subsequently resonantly convert into regular photons, $A' \rightarrow \gamma$, with kinetic mixing parameter ϵ when their mass matches the photon plasma mass $m_\gamma(\vec{x}, z)$ [27–29]. m_a , $m_{A'}$, τ_a , and ϵ are the free parameters in the model. The conversion results in a sharp increase in the number density of photons in the RJ tail of the CMB, which contribute to the 21-cm background photon temperature. The redshift of this feature, which we call an “edge,” is around

$$z_{\text{edge}} = z_{\text{res}}; \quad \overline{m_\gamma(z_{\text{res}})} = m_{A'}, \quad (1)$$

where z_{res} is the resonance redshift at which the plasma and dark photon masses match and $\overline{m_\gamma(z_{\text{res}})}$ is the mean plasma mass at that redshift, roughly related to the cosmological free electron number density $\overline{n_e(z)}$ by $\overline{m_\gamma(z)}^2 \approx 4\pi\hbar^2 e^2 \overline{n_e(z)} / (m_e c^4)$. This results in a near-instantaneous increase in the effective photon temperature, (further) decoupling the spin and photon temperatures, a consequence of which is an enhancement of the 21-cm brightness absorption feature. Measuring the location of the edge uniquely determines the dark photon mass, through Eq. (1).

Photons resonantly produced at a given redshift z_{res} and frequency ω_{res} then evolve to contribute to the number density of 21-cm photons at a given redshift z_{21} as $\omega_{\text{res}}(1+z_{21}) = \omega_{21}(1+z_{\text{res}})$. Kinematically, $\hbar\omega_{\text{res}} > m_a c^2 / 2$ is forbidden for a two-body decay, resulting in a spectral feature, which we call an “end point,” beyond which all of the converted photons have redshifted below the 21-cm frequency. The location of the end point z_{end} is defined through

$$\frac{1+z_{\text{end}}}{1+z_{\text{res}}} = \frac{\omega_{21}\hbar}{m_a c^2 / 2}. \quad (2)$$

Measuring the location of the edge uniquely determines $m_{A'}$ through Eq. (1), and measuring the end point location additionally specifies m_a through Eq. (2).

We note that the edges and end points that we identify in 21 cm are analogs to the edges and end points that can signify new physics in kinematic distributions at high energy colliders [30]. In both cases, these distinctive spectral features serve as handles to distinguish new physics from backgrounds.

For the remainder of this Letter we assume that a is the DM. The differential number density of dark photons of angular frequency ω at redshift z due to a decays is given by [19,31,32]

$$\frac{dn_{A'}}{d\omega} = \frac{2\rho_{\text{DM}}(z_{\text{dec}})(1+z)^3}{\tau_a H(z_{\text{dec}})m_a \omega(1+z_{\text{dec}})^3} \Theta\left(\frac{m_a c^2}{2\hbar} - \omega\right), \quad (3)$$

where z_{dec} is the redshift at which the decay $a \rightarrow A'A'$ takes place, $H(z_{\text{dec}})$ the Hubble rate and $\rho_{\text{DM}}(z_{\text{dec}})$ the DM

density, both evaluated at z_{dec} . Equation (3) presumes two-body decay kinematics with $\tau_a \gg t_U$, and takes $m_a \gg m_{A'}$. Note that for a two-body decay there exists a unique relation $z_{\text{dec}} = m_a c^2 / (2\hbar\omega) - 1$ between angular frequency and redshift of decay. The photon abundance $dn_\gamma/d\omega$ is obtained by multiplying $dn_{A'}/d\omega$ by the total $A' \rightarrow \gamma$ conversion probability $\langle P_{\gamma \rightarrow A'} \rangle = \int_{z_{\text{dec}}}^{z_{\text{edge}}} dz' d\langle P_{\gamma \rightarrow A'} \rangle / dz'$, computed following Refs. [28,29] and accounting for effects of inhomogeneities in the plasma mass. The existence of inhomogeneities in the photon plasma broadens the characteristic width of the spectral edge, since resonant conversions can now take place over some range of redshifts around z_{edge} [28,29,32–34]. Since this modifies the redshift at which the wavelength of produced photons redshifts beyond 21 cm, the end point acquires a characteristic width as well. Nevertheless, the redshift width of conversions considered here is much smaller than the sensitivities of relevant experiments [29], allowing the spectral features to be resolved. We use the fiducial setup from Ref. [28], with a log-normal description of plasma mass fluctuations and a simulation-inferred fluctuation spectrum [29] to compute conversion probabilities accounting for plasma mass perturbations. As in Ref. [28], we only consider plasma mass perturbations in the range $10^{-2} < 1 + \delta < 10^2$ throughout this work, since the log-normal distribution of perturbations cannot be assumed to be reliable outside of this range [28,29].

The effective 21-cm photon temperature including the excess photons $n_{A' \rightarrow \gamma}$ is computed as $T_\gamma(z) = T_{\text{CMB}}(z)(1 + n_{A' \rightarrow \gamma}/n_{\text{CMB}})$, where $T_{\text{CMB}}(z)$ is the standard CMB temperature and n_{CMB} the standard CMB number density corresponding to 21 cm. This effective 21-cm temperature is

shown in the left panel of Fig. 1 for an illustrative signal point with dark photon mass $m_{A'} = 10^{-12}$ eV, DM mass $m_a = 5.1 \times 10^{-5}$ eV, and kinetic mixing $\epsilon = 10^{-9}$. This corresponds to resonant conversion around $z_{\text{res}} \simeq 220$ and a kinematic end point around $z_{\text{end}} \simeq 50$.

Several constraints on this parameter space apply— (i) constraints from stellar energy loss due to $A'a$ pair production [19,38], (ii) constraints on excess $A' \rightarrow \gamma$ photon flux from radio and microwave observations [36,37], (iii) constraints on $\gamma \leftrightarrow A'$ from COBE/FIRAS [28,35], (iv) bounds on the DM lifetime τ_a , and (v) constraints from measurements of 21-cm emission at $z \sim 9$ –14 from EDGES high band [39]. The DM lifetime throughout this study is chosen to saturate the allowed bound [40]. The right panel of Fig. 1 shows the present-day number density spectrum of dark photons (dashed blue) and photons (solid red) compared to the standard CMB expectation (dotted green), along the measured values from COBE/FIRAS [35], ARCADE2 [36], and LWA radio surveys [37] for the illustrative parameter point. It can be seen that the photon spectrum in this case runs up against the measured radio flux at $\omega \simeq 2 \times 10^{-6}$ eV, constraining the maximum allowed injection. We note that late-time resonances (Fig. 1, left) are generically expected when conversions in overdense or underdense plasma regions can take place (for $m_{A'} \lesssim 3 \times 10^{-12}$ eV in our fiducial description of fluctuations) [28,29]. We have verified that, in these cases, the present-day radio flux [37] is far more constraining than EDGES high-band 21-cm measurements [39].

Such an enhancement in the 21-cm photon temperature is allowed by current constraints and can lead to striking signatures observable by current and future 21-cm and

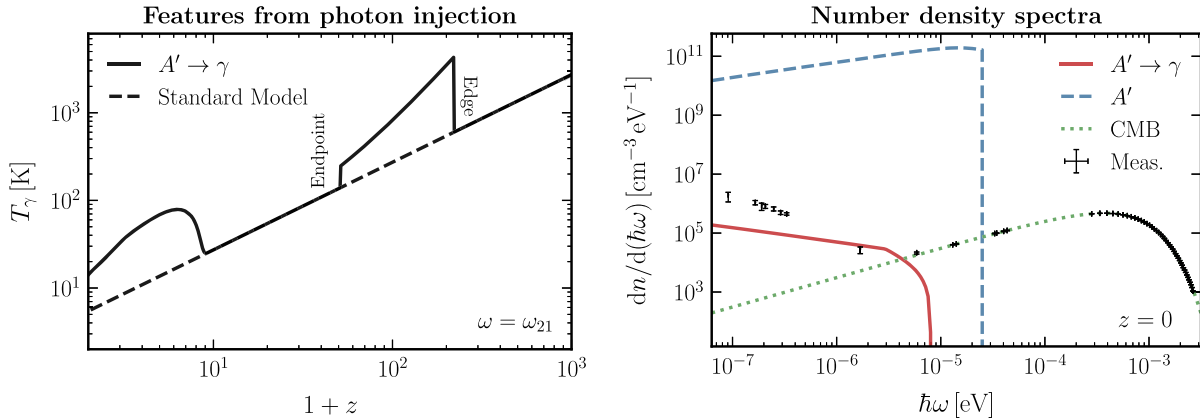


FIG. 1. (Left) Evolution of the 21-cm photon temperature for the standard case (dashed black) and including photon injection for an illustrative parameter point with dark photon mass $m_{A'} = 10^{-12}$ eV, DM mass $m_a = 5.1 \times 10^{-5}$ eV, and kinetic mixing $\epsilon = 1.4 \times 10^{-9}$. A sharp increase in effective temperature at $z \simeq 220$ followed by a turn-off at $z \simeq 50$ (corresponding to the regime where all injected photons have redshifted below 21 cm) can be seen, along with additional resonant injection at lower redshifts $z \lesssim 10$. (Right) For the same parameter point, the present-day differential number density spectra for dark photons (dashed blue), corresponding resonantly injected photons (solid red), and the standard CMB (dashed green) along with measurements from COBE/FIRAS [35], ARCADE2 [36], and LWA radio surveys [37] (black data points). A large excess in the photon number density in the RJ tail is consistent with observations of the CMB spectrum.

radio surveys, opening up a new avenue for probing the dark sector.

Applications to 21-cm observations.—The excess photon flux and, consequently, higher effective temperature resulting from resonant photon injection can leave characteristic imprints on the observed 21-cm signal. We focus on two benchmark scenarios here in order to illustrate the main qualitative features and relevance to current and future 21-cm measurements.

Benchmark 1: Spectral end point at $z \sim 15$ —A sharp turn-off in the photon temperature evolution due to a spectral end point will decrease the contrast between the spin and photon temperatures, turning off the 21-cm absorption feature. This parameter point corresponds to dark photon mass $m_{A'} = 10^{-11}$ eV, DM mass $m_a = 4.9 \times 10^{-4}$ eV, and kinetic mixing $\epsilon = 5 \times 10^{-8}$, which would result in resonant conversion around $z_{\text{edge}} \simeq 660$ and an end point around $z_{\text{end}} \simeq 15$.

Benchmark 2: Spectral features during the dark ages $z \sim 50$ – 95 —An edge or end point during the dark ages would result in a spectral feature potentially detectable with proposed space-based 21-cm measurements [23–25]. This parameter point corresponds to dark photon mass $m_{A'} = 2.5 \times 10^{-13}$ eV, DM mass $m_a = 1.7 \times 10^{-5}$ eV, and kinetic mixing $\epsilon = 4.5 \times 10^{-10}$, which would result in an edge around $z_{\text{edge}} \simeq 95$ and a kinematic end point around $z_{\text{end}} = 65$.

The evolution of the kinetic, photon, and spin temperatures for benchmarks 1 and 2 is shown in the left and right panels of Fig. 2, respectively. We employ the toy model for Lyman- α and x-ray heating [41] with additional input from Refs. [42–45] to compute the temperature evolution; details of our global 21-cm computation are described in the Supplemental Material [46]. A halo virial temperature cut $T_{\text{vir}} = 2 \times 10^4$ K and star-formation efficiency $f_* = 3\%$ is assumed by default, with the effective

x-ray star-formation efficiency for benchmark 1 lowered to 1% to demonstrate the effect of the spectral end point. For comparison, we also show results for a purely phenomenological power-law photon injection, $T_\gamma = T_{\text{CMB},0}(1+z) \times [1 + f_r A_r (\nu_0/78 \text{ MHz})^\beta]$ (dotted, labeled “power law”), where ν_0 is the present-day photon frequency, and A_r and β are motivated by and fit to the excess low-frequency radio background measured by ARCADE2 [36] and LWA [37] for $f_r = 1$ as in Refs. [10,47]. If some fraction f_r of this background is produced primordially, it can show up as a detectable signal in global 21-cm experiments. When comparing to benchmark 1, we set $f_r = 2\%$ in order to obtain an absorption depth consistent with the fiducial EDGES measurement. When comparing to benchmark 2 on the other hand, $f_r = 0.01\%$ of the radio emission is chosen to illustrate its signature during the dark ages and compare with the resonant photon injection scenario. We can see that spectral edges and end points would be clearly distinguishable from such astrophysical contributions.

The 21-cm brightness temperature corresponding to these scenarios is shown in Fig. 3. The left panel shows a signal with a spectral end point at $z \simeq 15$ (with parameters as in benchmark 1, red line) and lowered x-ray heating alongside the tentative EDGES measurement (blue band). The sharp turn-off in the absorption feature is now predominantly due to the spectral end point. For comparison, the case of power law photon injection is shown, with the turn-off due to x-ray heating. The Supplemental Material [46] further explores the viable parameter space within the model considered here that could contribute to the absorption feature observed by EDGES.

The right panel shows the effect of an injection around $z \sim 95$ and a kinematic end point at $z \sim 65$, corresponding to our benchmark 2 parameter point. The 15 mK uncertainty projected by the proposed DAPPER experiment in the 15–40 MHz frequency range [24] is shown as the green

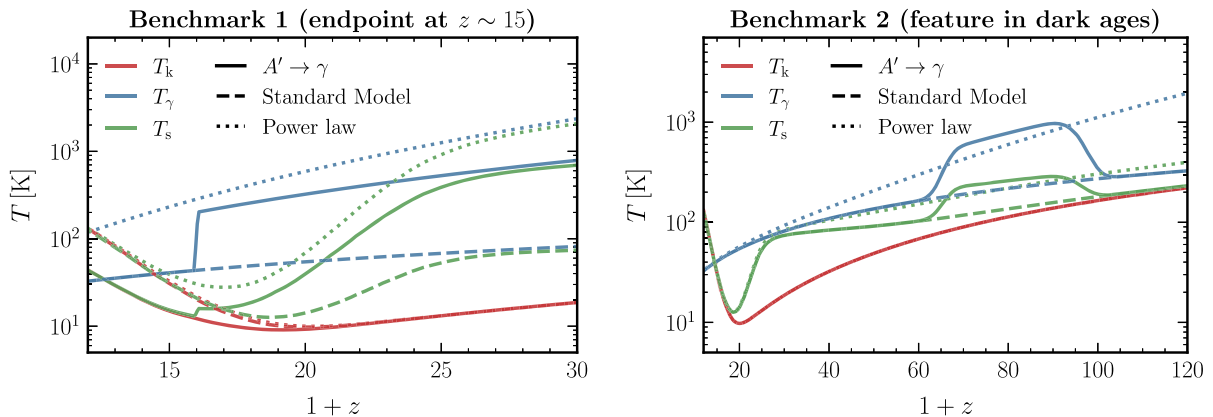


FIG. 2. Evolution of the kinetic (red), photon (blue), and spin (green) temperatures with redshift, shown for the standard model (dashed), phenomenological power law photon injection (dotted), and photon injection due to dark photon resonant conversion $A' \rightarrow \gamma$ (solid) shown for benchmark 1 (left) and benchmark 2 (right). Compared to the standard model and power law cases, reduced x-ray heating is assumed for the $A' \rightarrow \gamma$ scenarios.

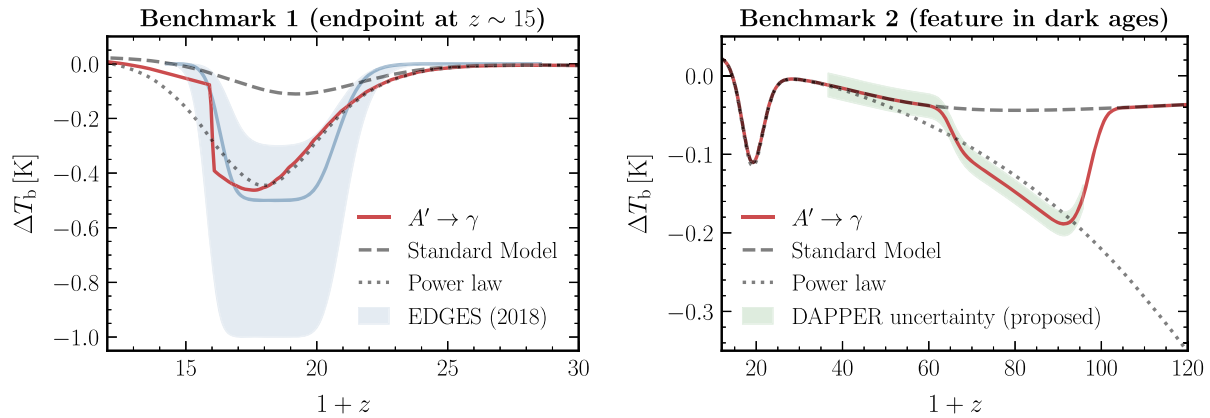


FIG. 3. The 21-cm brightness temperature contrast relative to the microwave background (solid red) for the benchmark scenarios considered: (left) Benchmark 1, showing a kinematic end point at $z = 15$ and resulting in a sharp turnoff in the absorption feature that could explain the EDGES measurement (blue band), and (right) benchmark 2, showing a distinctive kinematic feature during the dark ages. The expected 15 mK uncertainty of the space-based DAPPER experiment in the 15–40 MHz range [24] is illustrated as the green band in the right plot, showing that proposed space-based 21-cm experiments would be sensitive to such injections scenarios. The brightness temperature for the standard model expectation (dashed gray) and a phenomenological power law modification to the CMB temperature fit to low-frequency radio surveys (dotted gray) are shown for comparison.

band. It can be seen that such a distinctive spectral feature would be observable by future 21-cm experiments and easily distinguished from astrophysical backgrounds, providing a new probe of the nature of the dark sector.

Conclusions.—We have introduced a qualitatively new class of global 21-cm signatures resulting from interactions between the standard and dark sectors, characterized by spectral features—edges and end points—and excesses in the observed 21-cm global signal brightness temperature. We have shown how features resulting from dark photon-to-photon conversion can modify the 21-cm absorption trough during cosmic dawn, providing a potential explanation for the anomalous depth and shape of the 21-cm absorption feature measured by EDGES and, more generally, a new way to look for new physics in current and upcoming 21-cm measurements targeting the cosmic dawn era. We have additionally demonstrated how resonant photon injection can result in distinctive spectral features in the brightness temperature during the dark ages, which can be targeted by proposed space-based 21-cm experiments [23–25].

Although we have focused on a particular model realization here, we emphasize the generality of the signatures introduced. Any exotic resonant photon injection—such as due to conversions between SM photons and axionlike particles [20,21]—may generically result in a spectral edge in the 21-cm temperature. A kinematic end point in the model will correspondingly produce a spectral end point, which may be hard—as in the case of two-body decay considered here—or soft, as expected for three (or more)-body decay.

We have also focused exclusively on signatures in the *global* 21-cm signal; the inhomogeneous nature of resonant photon injection [29] implies that striking signatures may be expected in the 21-cm power spectrum as well, which is

expected to be targeted by ongoing and proposed surveys. We defer these additional applications of our framework to future work.

We thank Yacine Ali-Haïmoud, Misha Ivanov, Julien Lesgourgues, Julian Muñoz, Josef Pradler, Roman Scoccimarro, and Tejaswi Venumadhav for helpful conversations. A. C. acknowledges support from the “Generalitat Valencian” (Spain) through the “plan GenT” Program No. (CIDEAGENT/2018/019), as well as national Grants No. FPA2014-57816-P, FPA2017-85985-P, and the European Project No. H2020-MSCA-ITN-2015//674896-ELUSIVES. H. L. is supported by the DOE under Contract No. DESC0007968. S. M. and J. T. R. are supported by the NSF CAREER Grant No. PHY-1554858 and NSF Grant No. PHY-1915409. S. M. is additionally supported by the Simons Foundation. J. T. R. is also supported by a grant from the Alexander von Humboldt Foundation and by the Deutsche Forschungsgemeinschaft (DFG, German Research Foundation) under Germanys Excellence Strategy EXC 2121 Quantum Universe 390833306. J. T. R. acknowledges hospitality from the Aspen Center for Physics, which is supported by the NSF Grant No. PHY-1607611. M. P. is supported in part by U.S. Department of Energy (Grant No. desc0011842). A. U. is supported in part by the MIUR under Contract No. 2017 FMJFMW and by the INFN grant SESAMO. This work made use of the NYU IT High Performance Computing resources, services, and staff expertise. The authors are pleased to acknowledge that the work reported on in this Letter was substantially performed using the Princeton Research Computing resources at Princeton University which is a consortium of groups including the Princeton Institute for Computational Science and

Engineering and the Princeton University Office of Information Technology's Research Computing department. This research has made use of NASA's Astrophysics Data System. This research made use of the `ares` [52], `astropy` [62,63], `CAMB` [64,65], `CLASS` [66], `COLOSSUS` [53], `HyRec` [67], `IPYTHON`[68], `Jupyter` [69], `DarkHistory` [70], `MATPLOTLIB` [71], `nbodykit` [72], `NumPy` [73], `seaborn` [74], `pandas` [75], `SciPy` [76], and `tqdm` [77] software packages.

* andrea.caputo@uv.es

† hongwanl@princeton.edu

‡ sm8383@nyu.edu

§ ruderman@nyu.edu

|| alfredo.urban@sisssa.it

- [1] S. A. Wouthuysen, *Astron. J.* **57**, 31 (1952).
 [2] G. B. Field, *Astrophys. J.* **129**, 536 (1959).
 [3] J. D. Bowman, A. E. E. Rogers, R. A. Monsalve, T. J. Mozdzen, and N. Mahesh, *Nature (London)* **555**, 67 (2018).
 [4] R. F. Bradley, K. Tauscher, D. Rapetti, and J. O. Burns, *Astrophys. J.* **874**, 153 (2019).
 [5] B. T. Draine and J. Miralda-Escudé, *Astrophys. J. Lett.* **858**, L10 (2018).
 [6] R. Hills, G. Kulkarni, P. D. Meerburg, and E. Puchwein, *Nature (London)* **564**, E32 (2018).
 [7] M. Spinelli, G. Bernardi, and M. G. Santos, *Mon. Not. R. Astron. Soc.* **489**, 4007 (2019).
 [8] P. H. Sims and J. C. Pober, *Mon. Not. R. Astron. Soc.* **492**, 22 (2020).
 [9] S. Singh and R. Subrahmanyam, *Astrophys. J.* **880**, 26 (2019).
 [10] C. Feng and G. Holder, *Astrophys. J.* **858**, L17 (2018).
 [11] R. Barkana, *Nature (London)* **555**, 71 (2018).
 [12] A. Berlin, D. Hooper, G. Krnjaic, and S. D. McDermott, *Phys. Rev. Lett.* **121**, 011102 (2018).
 [13] R. Barkana, N. J. Outmezguine, D. Redigolo, and T. Volansky, *Phys. Rev. D* **98**, 103005 (2018).
 [14] S. Fraser *et al.*, *Phys. Lett. B* **785**, 159 (2018).
 [15] J. B. Muñoz and A. Loeb, *Nature (London)* **557**, 684 (2018).
 [16] A. A. Kurov, T. Venumadhav, L. Dai, and M. Zaldarriaga, *Astrophys. J.* **864**, L15 (2018).
 [17] J. Mirocha and S. R. Furlanetto, *Mon. Not. R. Astron. Soc.* **483**, 1980 (2019).
 [18] H. Liu, N. J. Outmezguine, D. Redigolo, and T. Volansky, *Phys. Rev. D* **100**, 123011 (2019).
 [19] M. Pospelov, J. Pradler, J. T. Ruderman, and A. Urbano, *Phys. Rev. Lett.* **121**, 031103 (2018).
 [20] T. Moroi, K. Nakayama, and Y. Tang, *Phys. Lett. B* **783**, 301 (2018).
 [21] K. Choi, H. Seong, and S. Yun, *Phys. Rev. D* **102**, 075024 (2020).
 [22] B. Holdom, *Phys. Lett.* **166B**, 196 (1986).
 [23] M. A. Alvarez *et al.*, arXiv:1903.04580.
 [24] J. O. Burns *et al.*, arXiv:1902.06147.
 [25] L. Koopmans *et al.*, arXiv:1908.04296.
 [26] N. Aghanim *et al.* (Planck Collaboration), *Astron. Astrophys.* **641**, A6 (2020).
 [27] A. Mirizzi, J. Redondo, and G. Sigl, *J. Cosmol. Astropart. Phys.* **03** (2009) 026.
 [28] A. Caputo, H. Liu, S. Mishra-Sharma, and J. T. Ruderman, *Phys. Rev. Lett.* **125**, 221303 (2020).
 [29] A. Caputo, H. Liu, S. Mishra-Sharma, and J. T. Ruderman, *Phys. Rev. D* **102**, 103533 (2020).
 [30] I. Hinchliffe, F. E. Paige, M. D. Shapiro, J. Soderqvist, and W. Yao, *Phys. Rev. D* **55**, 5520 (1997).
 [31] Y. Cui, M. Pospelov, and J. Pradler, *Phys. Rev. D* **97**, 103004 (2018).
 [32] A. A. Garcia, K. Bondarenko, S. Ploeckinger, J. Pradler, and A. Sokolenko, *J. Cosmol. Astropart. Phys.* **10** (2020) 011.
 [33] K. Bondarenko, J. Pradler, and A. Sokolenko, *Phys. Lett. B* **805**, 135420 (2020).
 [34] S. J. Witte, S. Rosauero-Alcaraz, S. D. McDermott, and V. Poulin, *J. High Energy Phys.* **06** (2020) 132.
 [35] D. J. Fixsen, E. S. Cheng, J. M. Gales, J. C. Mather, R. A. Shafer, and E. L. Wright, *Astrophys. J.* **473**, 576 (1996).
 [36] D. J. Fixsen *et al.*, *Astrophys. J.* **734**, 5 (2011).
 [37] J. Dowell and G. B. Taylor, *Astrophys. J.* **858**, L9 (2018).
 [38] M. Haft, G. Raffelt, and A. Weiss, *Astrophys. J.* **425**, 222 (1994); **438**, 1017(E) (1995).
 [39] R. A. Monsalve, A. E. E. Rogers, J. D. Bowman, and T. J. Mozdzen, *Astrophys. J.* **847**, 64 (2017).
 [40] V. Poulin, P. D. Serpico, and J. Lesgourgues, *J. Cosmol. Astropart. Phys.* **08** (2016) 036.
 [41] C. M. Hirata, *Mon. Not. R. Astron. Soc.* **367**, 259 (2006).
 [42] T. Venumadhav, L. Dai, A. Kurov, and M. Zaldarriaga, *Phys. Rev. D* **98**, 103513 (2018).
 [43] S. Furlanetto and S. J. Stoeber, *Mon. Not. R. Astron. Soc.* **404**, 1869 (2010).
 [44] Y. Ali-Haïmoud, P. D. Meerburg, and S. Yuan, *Phys. Rev. D* **89**, 083506 (2014).
 [45] A. Mesinger, S. Furlanetto, and R. Cen, *Mon. Not. R. Astron. Soc.* **411**, 955 (2011).
 [46] See Supplemental Material at <http://link.aps.org/supplemental/10.1103/PhysRevLett.127.011102>, which additionally includes Refs. [42–45,47–61], for details of the prescription used to compute the global 21 cm, explore the parameter space that can explain the observed EDGES signal, and provide a calculation of the effect of correlations between closely separated decays and resonance.
 [47] A. Fialkov and R. Barkana, *Mon. Not. R. Astron. Soc.* **486**, 1763 (2019).
 [48] J. R. Pritchard and A. Loeb, *Phys. Rev. D* **78**, 103511 (2008).
 [49] S. Furlanetto and J. R. Pritchard, *Mon. Not. R. Astron. Soc.* **372**, 1093 (2006).
 [50] P. Madau, A. Meiksin, and M. J. Rees, *Astrophys. J.* **475**, 429 (1997).
 [51] J. R. Dormand and P. J. Prince, *J. Comput. Appl. Math.* **6**, 19 (1980).
 [52] J. Mirocha, *Mon. Not. R. Astron. Soc.* **443**, 1211 (2014).
 [53] B. Diemer, *Astrophys. J. Suppl.* **239**, 35 (2018).
 [54] G. Despali, C. Giocoli, R. E. Angulo, G. Tormen, R. K. Sheth, G. Baso, and L. Moscardini, *Mon. Not. R. Astron. Soc.* **456**, 2486 (2016).
 [55] V. Bromm, R. P. Kudritzki, and A. Loeb, *Astrophys. J.* **552**, 464 (2001).

- [56] J. Mirocha, R. H. Mebane, S. R. Furlanetto, K. Singal, and D. Trinh, *Mon. Not. R. Astron. Soc.* **478**, 5591 (2018).
- [57] A. Schneider, *Phys. Rev. D* **98**, 063021 (2018).
- [58] S. Mineo, M. Gilfanov, and R. Sunyaev, *Mon. Not. R. Astron. Soc.* **419**, 2095 (2012).
- [59] S. Mineo, M. Gilfanov, R. Sunyaev, B. Lehmer, and G. Morrison, *Mon. Not. R. Astron. Soc.* **437**, 1698 (2014).
- [60] M. Greiner and T. Enßlin, *Astron. Astrophys.* **574**, A86 (2015).
- [61] R. Barkana and A. Loeb, *Astrophys. J.* **626**, 1 (2005).
- [62] A. M. Price-Whelan *et al.*, *Astron. J.* **156**, 123 (2018).
- [63] T. P. Robitaille *et al.* (Astropy Collaboration), *Astron. Astrophys.* **558**, A33 (2013).
- [64] A. Lewis, A. Challinor, and A. Lasenby, *Astrophys. J.* **538**, 473 (2000).
- [65] A. Lewis and S. Bridle, *Phys. Rev. D* **66**, 103511 (2002).
- [66] D. Blas, J. Lesgourgues, and T. Tram, *J. Cosmol. Astropart. Phys.* **07** (2011) 034.
- [67] Y. Ali-Haïmoud and C. M. Hirata, *Phys. Rev. D* **83**, 043513 (2011).
- [68] F. Perez and B. E. Granger, *Comput. Sci. Eng.* **9**, 21 (2007).
- [69] T. Kluyver *et al.*, in *Positioning and Power in Academic Publishing: Players, Agents and Agendas* (IOS Press, 2016), <http://dx.doi.org/10.3233/978-1-61499-649-1-87>.
- [70] H. Liu, G. W. Ridgway, and T. R. Slatyer, *Phys. Rev. D* **101**, 023530 (2020).
- [71] J. D. Hunter, *Comput. Sci. Eng.* **9**, 90 (2007).
- [72] N. Hand, Y. Feng, F. Beutler, Y. Li, C. Modi, U. Seljak, and Z. Slepian, *Astron. J.* **156**, 160 (2018).
- [73] S. van der Walt, S. C. Colbert, and G. Varoquaux, *Comput. Sci. Eng.* **13**, 22 (2011).
- [74] M. Waskom *et al.*, mwaskom/seaborn: v0.8.1 (september 2017) (2017).
- [75] W. McKinney, in *Proceedings of the 9th PYTHON in Science Conference*, edited by S. van der Walt and J. Millman (2010), pp. 51–56, <https://conference.scipy.org/proceedings/scipy2010/>.
- [76] P. Virtanen *et al.*, *Nat. Methods* **17**, 261 (2020).
- [77] C. O. da Costa-Luis, *J. Open Source Softw.* **4**, 1277 (2019).